



**HAL**  
open science

## Sub-micrometric $\beta$ -CoMoO<sub>4</sub> rods: optical and piezochromic properties.

Veronica Blanco-Gutierrez, Alain Demourgues, Manuel Gaudon

### ► To cite this version:

Veronica Blanco-Gutierrez, Alain Demourgues, Manuel Gaudon. Sub-micrometric  $\beta$ -CoMoO<sub>4</sub> rods: optical and piezochromic properties.. Dalton Transactions, 2013, 42 (37), pp.13622-13627. 10.1039/c3dt51656c . hal-00861792

**HAL Id: hal-00861792**

**<https://hal.science/hal-00861792>**

Submitted on 12 Jul 2022

**HAL** is a multi-disciplinary open access archive for the deposit and dissemination of scientific research documents, whether they are published or not. The documents may come from teaching and research institutions in France or abroad, or from public or private research centers.

L'archive ouverte pluridisciplinaire **HAL**, est destinée au dépôt et à la diffusion de documents scientifiques de niveau recherche, publiés ou non, émanant des établissements d'enseignement et de recherche français ou étrangers, des laboratoires publics ou privés.

## Sub-micrometric $\beta$ -CoMoO<sub>4</sub> rods: optical and piezochromic properties

Veronica Blanco-Gutierrez, Alain Demourgues and Manuel Gaudon\*

Sub-micrometric  $\beta$ -CoMoO<sub>4</sub> rods have been obtained after thermal treatment of CoMoO<sub>4</sub>·H<sub>2</sub>O previously prepared by the precipitation method. The color of the sub-micrometric particles has been investigated through diffuse reflectance in the VIS-IR range and the spectra have been compared with those corresponding to samples with larger isotropic particles. The O<sup>2-</sup>→Mo<sup>6+</sup> charge transfer band shifts to the UV region with decreasing the particle size, revealing a more covalent bond. This can be justified under the consideration of a higher proportion of surface-atoms in sub-micrometric particles that present lower coordination number. The piezochromic behavior of the sub-micrometric  $\beta$ -CoMoO<sub>4</sub> rods has been investigated. As the sub-micrometric size of the particles stabilizes the low-coordination phase ( $\beta$ -phase), the transition pressure to the  $\alpha$ -phase is higher in comparison with that corresponding to larger particles. In addition, it was not possible to obtain a 100% transformation of the  $\beta$ -phase in the sample with sub-micrometric particles. A similar temperature influence on the transition pressure regardless of particle size has also been observed.

DOI:10.1039/XXXXXXXXXX

### Introduction

One of the most interesting physical properties exhibited by some inorganic materials is piezochromic behavior which consists of a color variation with pressure due to a phase-transition between two crystal structures.<sup>1-3</sup> Unlike the slight change of color that the oxides exhibit for instance with the thermal expansion/contraction, in the case of the piezochromic behavior a drastic color modification can be observed associated with a first order phase transition. Several AMoO<sub>4</sub> (A: Ni, Cu, Co, ...) molybdates exhibit piezochromic behavior<sup>4-6</sup> with a transition pressure ( $P_{tr}$ ) depending on the electronegativity of the A cation. Thus, the CoMoO<sub>4</sub> material exhibits at room temperature a  $P_{tr}$  around 35 bar which makes it a potential candidate to be used as a shock detector in several applications. This mixed oxide compound presents four allotropic forms, three of them stable at room pressure: CoMoO<sub>4</sub>·xH<sub>2</sub>O,  $\beta$ -CoMoO<sub>4</sub> and  $\alpha$ -CoMoO<sub>4</sub>, and the last one II-CoMoO<sub>4</sub>, only observable at very high pressure values.<sup>7,8</sup> The  $\beta$ -phase (high temperature, low pressure form) is the only one that presents piezochromic behavior to be transformed into the  $\alpha$ -phase (low temperature, high pressure form) with a change of color from purple to green.<sup>4</sup> Both the  $\beta$  and  $\alpha$  forms crystallize in the C2/m space group with the Co<sup>2+</sup> cations located in distorted octahedral sites. However, Mo<sup>6+</sup> cations change their

coordination from tetrahedral to octahedral site when going from  $\beta$  to  $\alpha$  form. As a consequence of the applied pressure, four isolated [MoO<sub>4</sub>] tetrahedra in the  $\beta$ -phase get linked by edge-sharing to give in the  $\alpha$ -phase a [Mo<sub>4</sub>O<sub>16</sub>] tetramer of octahedral atoms, with a consequent increase of the crystal density. On the other hand, the color for both phases can be described by two contributions, one corresponding to Co<sup>2+</sup> d-d transitions and a second one corresponding to the O<sup>2-</sup>→Mo<sup>6+</sup> charge transfer band (C.T.B.). When the  $\beta$ → $\alpha$  transition takes place, the Mo<sup>6+</sup> cations increase their coordination number with a consequent decreasing of the strength of the covalent Mo-O bond. This phenomenon results in a shift to the lower energy regions of the O<sup>2-</sup>→Mo<sup>6+</sup> C.T.B. and induces the green color of the  $\alpha$ -phase.<sup>4</sup>

Although the CoMoO<sub>4</sub> compound is easily prepared by the solid-state route, the soft-chemistry routes like co-precipitation, hydrothermal synthesis, or employment of micro-emulsions allow decreasing the preparation temperature and obtaining samples with different particle sizes and morphologies.<sup>9-11</sup> In addition, wet-chemistry processes in comparison with the solid-state route offer the possibility to reduce the particle dimensions up to the sub-micrometric scale with a homogeneous size and morphology.<sup>12-15</sup>

Here we report that in the case of cobalt molybdate preparation, the employment of the soft-chemistry route leads to the hydrate compound CoMoO<sub>4</sub>·xH<sub>2</sub>O instead of the  $\beta$ -phase. In the crystal structure of this phase, the Co<sup>2+</sup> and Mo<sup>6+</sup> cations are located in distorted octahedral and tetrahedral sites, respectively, like in the case of the  $\beta$ -phase.<sup>6,16,17</sup> However,

unlike the  $\beta$ -CoMoO<sub>4</sub> compound, the CoMoO<sub>4</sub>·*x*H<sub>2</sub>O does not present piezochromic properties. In order to obtain the  $\beta$ -phase able to transit with the pressure, a subsequent thermal treatment is necessary to dehydrate the mixed oxide. The optical properties of the sub-micrometric particles and the piezochromic behavior depending on the particle size and temperature have been investigated.

## Results

The study has been carried out considering five Co-molybdate samples with different sizes and morphologies labeled as: RH, R $\beta$ , R $\beta\alpha$ , C $\beta$  and C $\alpha$ , where R and C refer to the sub-micrometric rods and samples obtained through the ceramic method, respectively. H,  $\beta$  and  $\alpha$  refers to the hydrate,  $\beta$  and  $\alpha$  phases, respectively.

The dehydration process of RH sample was studied by TGA under air from room temperature up to 700 °C. Fig. 1 shows the TG curve together with its derivative DTG that indicates the thermodynamics of the process. Two well-defined dehydration steps can be observed with the temperature. As the DTG curve suggests, the first one occurs in a broad temperature range between 100 and 300 °C and the second one drastically takes place at 340 °C. The total 7.4% weight loss with 5.9 and 1.5% loss in the first and second steps, respectively, indicates an almost monohydrate compound CoMoO<sub>4</sub>·H<sub>2</sub>O instead of the CoMoO<sub>4</sub>·3/4H<sub>2</sub>O reported by other authors.<sup>9,16</sup> The two dehydration steps are related to the liberation of two different kinds of water molecules. According to the literature, those eliminated in the first step may correspond to adsorbed molecules entrapped in the cavities of the structure, and those released in the second step are structural units whose elimination leads to the hydrate→ $\beta$ -phase transformation.<sup>16,18</sup> Therefore, up to 300 °C, RH sample progressively loses the entrapped water in the structural cavities that represents 80% of the total mass loss, and at 340 °C the structural water is drastically eliminated leading to the  $\beta$ -phase.

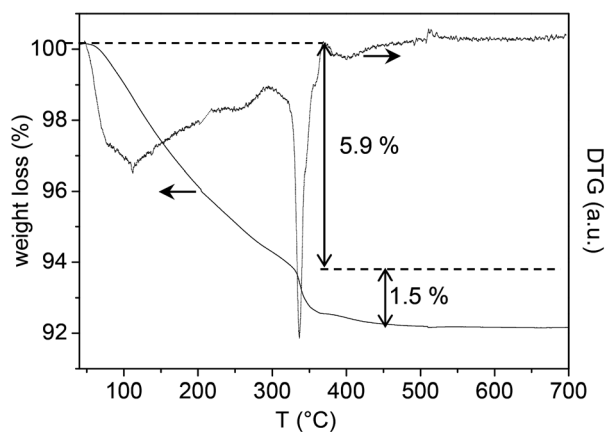


Fig. 1 TGA in air for the as-prepared CoMoO<sub>4</sub>·H<sub>2</sub>O precursor. DTG is also presented.

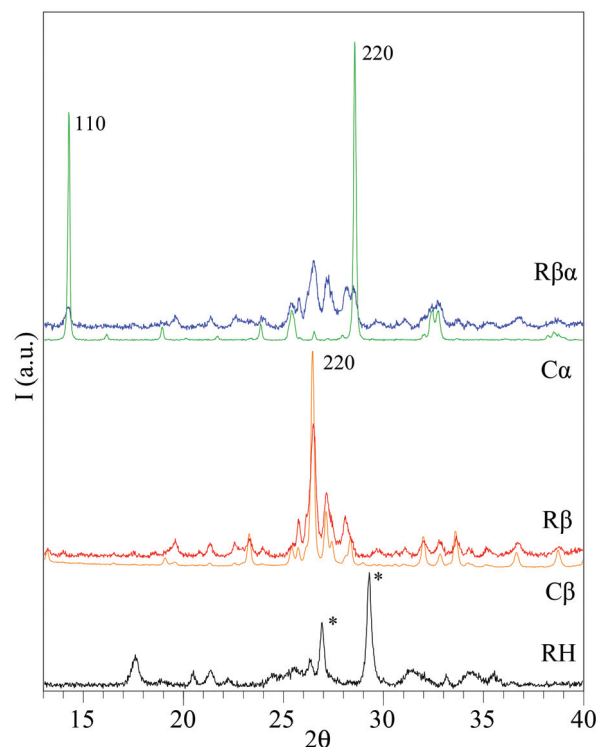


Fig. 2 X-ray diffraction patterns corresponding to RH, R $\beta$  and R $\beta\alpha$  samples. Patterns of C $\beta$  and C $\alpha$  samples are shown as a reference.

In Fig. 2 are shown the X-ray diffraction patterns corresponding to RH, R $\beta$  and R $\beta\alpha$  samples together with those corresponding to the samples obtained by the solid-state route C $\beta$  and C $\alpha$  that have been taken as reference compounds. The diffraction maxima corresponding to the pattern of RH sample can be indexed to the characteristic structure of the hydrate compound.<sup>16</sup> On the other hand, while the diffraction maxima of R $\beta$  sample can be ascribed to the  $\beta$ -phase as can be deduced by comparison with the pattern corresponding to C $\beta$  sample, in the case of R $\beta\alpha$  sample, the diffractogram can be ascribed to both  $\beta$  and  $\alpha$  structural phases revealing that it was not possible to achieve by grinding the total phase transformation to the high-pressure form. This is in accordance with the already known stabilization of the low-coordination phase ( $\beta$  form) with decreasing the particle size.<sup>19</sup> When the particle size gets reduced, the surface to volume ratio increases and the rate of surface atoms that present lower coordination becomes more important.

On the other hand, the patterns corresponding to RH, R $\beta$  and R $\beta\alpha$  samples exhibit broad diffraction peaks revealing a small crystal domain size, which in addition has been estimated by the Scherrer equation<sup>20</sup>:

$$D = \frac{0.9\lambda}{\beta \cos \theta}$$

where  $\lambda = 1.54056 \text{ \AA}$  corresponds to the Cu K $\alpha$  radiation, and  $\beta$  is the full width at half-maximum for a diffraction peak located at  $2\theta$ . *D* values of  $30 \pm 7$ ,  $25 \pm 5$  and  $27 \pm 6$  nm

corresponding to RH, R $\beta$  and R $\beta\alpha$  samples, respectively, were noted. For the  $D$  estimation, the diffraction peaks located at  $2\theta$  values of 17.6, 26.5 and 14.2 for RH, R $\beta$  and R $\beta\alpha$  samples, respectively, have been considered. Therefore, in the case of R $\beta\alpha$  sample, the calculated  $D$  value corresponds to the  $\alpha$ -phase. On the other hand, in the case of RH sample the presence of two sharp diffraction peaks (marked with \* in Fig. 2) in comparison with the rest of the diffractogram may indicate an anisotropic particle shape.

Fig. 3 shows representative TEM images of C $\beta$ , RH and R $\beta$  samples. As can be seen, while in the case of the C $\beta$  sample the solid-state route leads to particles with an irregular shape and dimensions larger than 2  $\mu\text{m}$  (Fig. 3a), in the case of RH and R $\beta$  samples the precipitation method allows not only to decrease the particle size (below 2  $\mu\text{m}$ ) but also to obtain a regular morphology (Fig. 3b–3f). Well-defined sub-micrometric CoMoO $_4$ ·H $_2$ O rods were obtained with a diameter between 200 and 400 nm and a length over 1  $\mu\text{m}$  (Fig. 3b–3d). This morphology is related to an intrinsic structural anisotropy<sup>21</sup> that induces particle growth along one of the axes in accordance with the X-ray diffraction patterns of the RH sample. However, the high temperature value employed in the ceramic route causes the sintering process to override the particle growth in a preferred orientation, resulting in an irregular morphology (see the TEM image of the C $\beta$  sample in Fig. 3a). On the other hand, the thermal treatment employed in the dehydration

process allows preserving the morphology of the precursor in the sub-micrometric  $\beta$ -CoMoO $_4$  sample according to a topotactic transition, with no traces of sintering (see TEM images Fig. 3e and 3f). It is worth mentioning as well the rough surface that R $\beta$  particles present in comparison with the RH sample as a consequence of the dehydration process. On the other hand, TEM images reveal significantly larger particle dimensions in the case of RH and R $\beta$  samples than the crystal domain sizes estimated by X-ray diffraction. This clearly indicates that the sub-micrometric rods are composed of thinner units of nanometric diameter as can be visualized in the case of R $\beta$  sample thanks to the dehydration process.

The diffuse reflectance spectra and their Kubelka–Munk transformation of C $\beta$ , C $\alpha$ , RH and R $\beta$  and R $\beta\alpha$  samples are presented in Fig. 4a and 4b, respectively. The spectra depicted in Fig. 4a can be described by two optical contributions, a typical d–d absorption band assigned to Co $^{2+}$  in octahedral sites together with an absorption threshold attributed to a charge transfer band from O $^{2-}$ →Mo $^{6+}$ .<sup>4</sup> As has been already reported, the K/S spectra in the VIS-IR range shows three spin allowed d–d transitions, namely  $^4T_{1g}$ → $^4T_{2g}(F)$ ,  $^4T_{1g}$ → $^4A_{2g}(F)$  and  $^4T_{1g}$ → $^4T_{1g}(P)$ , and three extra bands that are very convoluted, assigned to forbidden d–d transitions between doublet and quadruplet states (see Fig. 4a).<sup>4</sup> Although the three phases

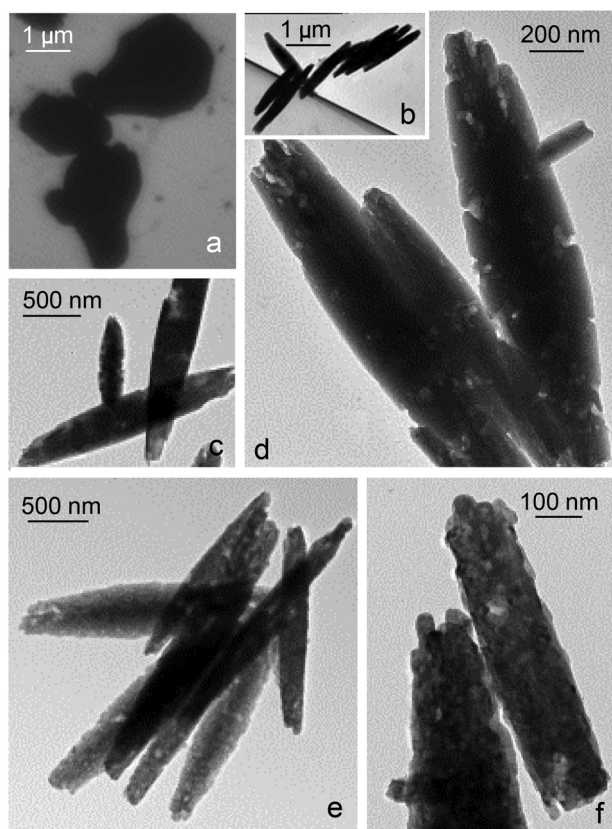


Fig. 3 TEM images corresponding to C $\beta$  (a), RH (b–d) and R $\beta$  (e and f) samples.

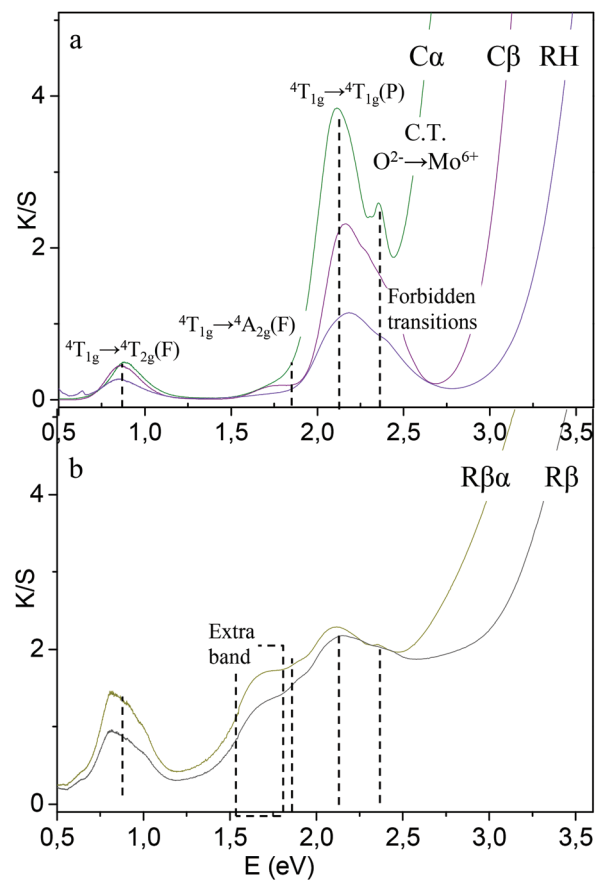


Fig. 4 K/S (Kubelka–Munk transformation) spectra for C $\alpha$ , C $\beta$ , RH samples (a) and R $\beta\alpha$  and R $\beta$  samples (b).

present the same absorbing d-d band because the  $\text{Co}^{2+}$  cations are located in octahedral sites in all the cases, a shift of the C.T.B. to the UV region can be observed when going from the  $\alpha$  to  $\beta$  and hydrate phases. The  $\text{O}^{2-} \rightarrow \text{Mo}^{6+}$  C.T.B. shifts from 2.4 ( $\alpha$ -phase) to 2.9 eV ( $\beta$ -phase). This has been attributed to a different sphere coordination in the  $\text{Mo}^{6+}$  cations depending on the crystal structure. Thus, while in the case of the  $\alpha$ -phase the  $\text{Mo}^{6+}$  cations are located in octahedral sites, when it comes to the  $\beta$  one, they present tetrahedral coordination. The reduction of the coordination number leads to a bond valence increment with the consequent more covalent Mo-O bond, which would be in accordance with a higher energy of the  $\text{O}^{2-} \rightarrow \text{Mo}^{6+}$  charge transfer. Following this reasoning, it could be said that the hydrate phase is the one that presents the most covalent Mo-O bond as its C.T.B. is located at 3.1 eV. It has been already reported that  $\text{Mo}^{6+}$  cations exhibit tetrahedral coordination in both  $\beta$  and hydrate phases.<sup>16,17</sup> On the other hand, when it comes to small particles, due to an increment of the surface to volume ratio, the surface-atoms play an important role in the properties of these sub-micrometric scaled materials. It is well known that the surface-atoms are characterized by the lowest coordination number which would decrease the overall coordination of the  $\text{Mo}^{6+}$  cations in the material, and therefore, the covalent Mo-O bond would be generally stronger. In addition, the presence of water molecules in the vicinity of  $\text{Co}^{2+}$  contributes, by the competitive bonds effect, to the strength of this covalent bond. This would justify the shift of the  $\text{O}^{2-} \rightarrow \text{Mo}^{6+}$  C.T.B. to higher energy regions in the case of the hydrate phase. Hence, as  $\text{C}\alpha$ ,  $\text{C}\beta$  and RH samples present the same d-d transition band, the different colors they exhibit can be explained by considering the C.T.B. position related to the strength of the covalent Mo-O bond. While in the case of the  $\alpha$ -phase the C.T.B. absorbs in the green-blue region, in the case of the  $\beta$  and hydrate phases, it is displaced to the violet region. The different purple color between the  $\beta$ -phase with larger particle size and the hydrate phase with smaller particle size is due to a displacement of the C.T.B. to higher energy regions in the case of the sub-micrometric particles. On the other hand, a decreasing of the K/S intensity of the  $\text{Co}^{2+}$  d-d bands from  $\text{C}\alpha$  to RH sample can be observed in Fig. 4a. Two factors influence the K/S intensity: (1) a distortion of the symmetry of the site where the chromophore cation is placed. Thus, the higher the distortion, the higher the intensity observable in the spectra. (2) The refractive index which depends on the composition and the crystal density. For a same  $\text{CoMoO}_4$  composition in the case of  $\text{C}\alpha$  and  $\text{C}\beta$  samples, the lower K/S intensity exhibited by  $\text{C}\beta$  sample may be in accordance with a lower crystal density of 4.57 instead of 4.78  $\text{g cm}^{-3}$  for the  $\alpha$ -phase<sup>16</sup> and more distorted oh-sites in the case of  $\text{C}\alpha$  sample. In this sense, RH sample presents the lowest K/S intensity related to a lower refractive index due to its more ionic structure thanks to water groups and a much lower density of 3.76  $\text{g cm}^{-3}$ ;<sup>16</sup> also the probably not so distorted octahedral sites in the case of RH sample may contribute to the lowering of the intensity corresponding to d-d transition bands in this sample.

On the other hand, the spectra corresponding to  $\text{R}\beta$  and  $\text{R}\beta\alpha$  samples illustrate the two already mentioned optical contributions ( $\text{Co}^{2+}$  d-d bands and  $\text{O}^{2-} \rightarrow \text{Mo}^{6+}$  C.T.B.) together with an extra band appearing at 1.50–1.75 eV (Fig. 4b). This may indicate a new coordination sphere for  $\text{Co}^{2+}$  that probably corresponds to those cations previously coordinated to water molecules. Thus, some structural defects may have been created during the dehydration process resulting in a new “metastable” coordination geometry that would suppose the appearance of a non-centrosymmetric site, allowing the d-d transitions to be observable by Laporte rules. This would be in accordance with the non-appearance of this extra band in the RH sample spectrum. The shift to high energy regions of the  $\text{O}^{2-} \rightarrow \text{Mo}^{6+}$  C.T.B. that the spectra of  $\text{R}\beta$  and  $\text{R}\beta\alpha$  samples illustrate in comparison with  $\text{C}\beta$  and  $\text{C}\alpha$  samples is in accordance with the already explained more stronger covalent Mo-O bond in these sub-micrometric particles.

Fig. 5 presents the variation of phase transition with pressure at room temperature and 100 °C corresponding to the  $\beta$ -phase of the  $\text{CoMoO}_4$  compound with micrometric and sub-micrometric particle size (Fig. 5a and 5b,  $\text{C}\beta$  and  $\text{R}\beta$  samples, respectively). The phase transition has been depicted after normalization of the  $\alpha/\beta$  phase ratio associated with the  $a^*$  color parameter variation with pressure.<sup>19</sup> From this curve, the transition pressure ( $P_{\text{tr}}$ ) value which corresponds to 50% of the  $\beta$  to  $\alpha$  phase transition can be estimated. As has been already seen from XRD, in the case of the sample composed of

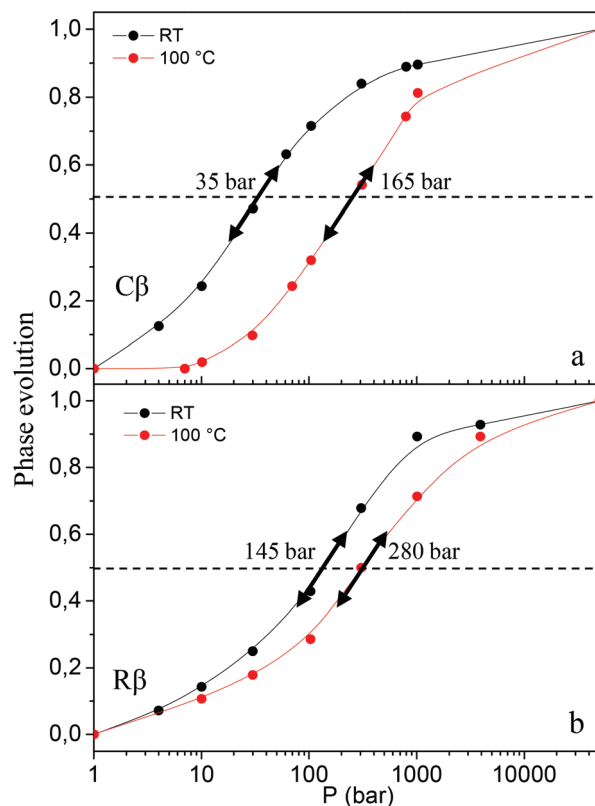


Fig. 5 Phase transformation with pressure from the  $\beta$  to  $\alpha$  form at room temperature and 100 °C corresponding to  $\text{C}\beta$  (a) and  $\text{R}\beta$  (b) particles.

sub-micrometric particles (Fig. 5b), it is not possible to obtain a 100% transformation of the  $\beta$  phase into the  $\alpha$  one (see the XRD pattern of  $R\beta\alpha$  sample in Fig. 2). Therefore, the normalized curve has been done considering the  $a^*$  value for maximum transformation. The different  $P_{tr}$  values of 35 and 145 bar, corresponding to  $C\beta$  and  $R\beta$  samples, respectively, are in agreement with the already reported influence of the particle size on the transition pressure.<sup>19</sup> When the particles become smaller, the low-coordination  $\beta$ -phase is stabilized resulting in a delay of the transition with pressure. On the other hand, it can be observed that regardless of the particle size, a 75 °C increment in the temperature induces a  $\sim$ 130 bar displacement of the phase transition due to the competition between typical pressure contraction and volume expansion with temperature (compare Fig. 5a and 5b). The same temperature influence on the  $P_{tr}$  for both samples suggests that the linear dependence between both parameters for a typical phase transition indicated by

$$P = \alpha/\gamma(T_c^* - T_c)$$

(where  $\alpha$  and  $\gamma$  are parameters,  $T_c$  is the transition temperature and  $T_c^*$  is the normalized transition temperature) is preserved independently of the particle size.<sup>22</sup>

It is worth noting that the evolution curve of  $C\beta$  and  $R\beta$  samples presents a similar tendency as is indicated by the double-arrow in the graphs. The fact that two samples with very different particle size distributions illustrate such a similar shape for the evolution curve supports the already reported idea that the tendency of the curve is greatly dependent on the manner of pressure-application. Thus, a pressure-application in a uniaxial way is characterized by a standard Gaussian distribution of inter-grain contact areas in the pellet.<sup>19</sup> This phenomenon reported for large crystals could be extrapolated in the same magnitude for sub-micrometric particles justifying the same curve tendency irrespective of the particle size distribution.

## Experimental section

### Samples preparation

The study has been carried out considering five Co-molybdate samples with different sizes and morphologies: RH,  $R\beta$ ,  $R\beta\alpha$ ,  $C\beta$  and  $C\alpha$ .

The precipitation method was employed in order to synthesize  $\text{CoMoO}_4 \cdot \text{H}_2\text{O}$  with sub-micrometric particle size. All chemical reactants were purchased from Aldrich and used without further purification. The stoichiometric reaction was made with cobalt acetate and sodium molybdate as sources of  $\text{Co}^{2+}$  and  $\text{MoO}_4^{2-}$ , respectively. A  $4 \times 10^{-3}$  M solution of  $\text{Co}(\text{CH}_3\text{COO})_2 \cdot 4\text{H}_2\text{O}$  in ethanol and a  $2 \times 10^{-2}$  M solution of  $\text{Na}_2\text{MoO}_4$  in water were prepared. Afterwards, the sodium molybdate solution was added drop by drop and under stirring to the cobalt acetate one to obtain a purple precipitate. The mixture was stirred at room temperature for a maturation time of 12 h and the  $\text{CoMoO}_4 \cdot \text{H}_2\text{O}$  product, labeled as RH, was washed with ethanol and recovered by centrifugation. The

$\beta$ -phase ( $R\beta$  sample) was easily obtained after treating the RH precursor at 500 °C in air for 1 min. For this purpose, RH sample was placed in the furnace once the desired temperature was achieved and removed after 1 min treatment to let the sample cool down to room temperature. Afterwards, a portion of the  $R\beta$  sample was ground in agate mortar simulating a high pressure application and was labeled as  $R\beta\alpha$ .

The piezochromic properties of  $R\beta$  sample were compared with those corresponding to a cobalt molybdate compound with larger particle size prepared by the standard solid-state route (700 °C under air, 20 h). A portion of this sample named  $C\beta$  was ground in agate mortar to obtain the  $C\alpha$  sample.

### Characterization techniques

TGA analysis was performed in air on a Setsys CS EVO apparatus with a heating rate of 5 °C  $\text{min}^{-1}$ . The structural characterization was made by X-ray diffraction using a Philips PW 1820 apparatus equipped with a  $\text{K}\alpha_1/\text{K}\alpha_2$  source and a copper anticathode. Diffraction patterns were collected with a  $2\theta$  step of 0.02° between 20° and 40° with a counting rate of 10 s per step in the routine mode.

The microstructural characterization was performed by Transmission Electron Microscopy using a JEOL-2000FX microscope working at 200 kV and an LVMS microscope from Delong Instruments, working at 5 kV. Diffuse reflectance spectra  $R(\lambda)$  were recorded at room temperature using a Cary 17 spectrophotometer using an integration sphere in the 350–850 nm wavelength range with a 1 nm step and a 2 nm bandwidth. Halon was used as a white reference for the blank. On the other hand, visible–NIR spectroscopic analyses were carried out in Diffuse Reflectance mode with a Konica–Minolta CM-700d spectrophotometer equipped with an integrating sphere coated with polytetrafluoroethylene. Measurements were performed for wavelengths varying from 200 up to 2500 nm, in the Specular Component Excluded (SCE) mode. A white calibration cap CM-A177 (ceramic) was used as a white reference and the standard D65 (daylight, color temperature: 6504 K) with a 10° observer angle (CIE1964) as an illuminant. Only the UV–visible wavelength range and the  $La^*b^*$  space parameters ( $L$ , luminosity;  $a^*$ , the green to red axis; and  $b^*$ , yellow to blue axis coefficients) were considered. No computing mathematics treatment was performed since the apparatus directly sets  $La^*b^*$  chromatic parameters. The  $a^*$  colorimetric parameter is descriptive of the green–red hue axis. This parameter was chosen in order to quantify the  $\alpha$  and  $\beta$  forms ratio inside the powder sample during the phase transition since the  $a^*$  value is very different for the two allotropic forms,  $a^* = -3.1$  and  $+11.2$  for  $\alpha$  and  $\beta$ -forms, respectively.

Pressure was applied in a uniaxial way following the details described in a previous study.<sup>19</sup> The powder samples were introduced in a pellet matrix with a varying diameter from 6 to 13 mm depending on the desired pressure. The pressure was applied thanks to a home-built scalepan balance in which a counter mass was used in a lever system with a pivot point in order to multiply the mechanical force (effort) that can be applied on the piston of the pellet matrix.<sup>19</sup>

## Conclusions

Sub-micrometric  $\text{CoMoO}_4 \cdot \text{H}_2\text{O}$  rods have been prepared by a straightforward method employing the precipitation method. After a thermal treatment of the hydrate precursor it was possible to obtain the  $\beta$ -phase with the same morphology associated with a topotactic transformation and any indications of sintering. It has been found that sub-micrometric particles do not transit in total into the  $\alpha$ -phase due to the stabilization of the low-coordination form with the particle size reduction. Both the  $\beta$ -phase and hydrate compound present the  $\text{Co}^{2+}$  and  $\text{Mo}^{6+}$  located in octahedral and tetrahedral sites, respectively. However, by VIS-IR spectra, more covalent Mo–O bonds of RH, R $\beta$  and R $\beta\alpha$  samples could be deduced as the  $\text{O}^{2-} \rightarrow \text{Mo}^{6+}$  C.T.B. is shifted to higher energy regions in comparison with C $\beta$  and C $\alpha$  samples. The more covalent bond has been related to the sub-micrometric particle size for which surface atoms that present lower coordination become more important. In the case of RH sample, the presence of water molecules in the vicinity of  $\text{Co}^{2+}$  has also been taken into account. On the other hand, samples obtained after thermal treatment of the hydrate compound exhibit an extra band in their spectra that has been attributed to new coordination spheres of  $\text{Co}^{2+}$  related to the structural defects originating during the dehydration process. In the case of the phase evolution with pressure, it has been found a delay of the transformation in particles with sub-micrometric size and a similar tendency for the evolution curve regardless of the particle size distribution, as it is greatly dependent on the manner of pressure-application that is the same in both cases.

## Acknowledgements

The authors are thankful to the European Commission (FP7 programme) for financial support of the SARISTU project, Etienne Durand for technical support with the TGA measurement and Laure Rocheron for the TEM measurements.

## Notes and references

- M. Gaudon, P. Deniard, A. Demourgues, A.-E. Thiry, C. Carbonera, A. Le Nestour, A. Largeau, J.-F. Létard and S. Jobic, *Adv. Mater.*, 2007, **19**, 3517–3519.
- F. Rodriguez, D. Hernandez, J. Garcia-Jaca, H. Ehrenberg and H. Weitzel, *Phys. Rev. B: Condens. Matter*, 2000, **61**, 497–501.
- D. Hernandez, F. Rodriguez, J. Garcia-Jaca, H. Ehrenberg and H. Weitzel, *Physica B*, 1999, **265**, 181–185.
- L. C. Robertson, M. Gaudon, S. Jobic, P. Deniard and A. Demourgues, *Inorg. Chem.*, 2011, **50**, 2878–2884.
- M. Gaudon, A.-E. Thiry, A. Largeau, P. Deniard, S. Jobic, J. Majimel and A. Demourgues, *Inorg. Chem.*, 2008, **47**, 2404–2410.
- J. A. Rodriguez, S. Chaturvedi, J. C. Hanson and J. L. Brito, *J. Phys. Chem. B*, 1999, **103**, 770–781.
- C. Livage, A. Hynaux, J. Marrot, M. Nogues and G. Férey, *J. Mater. Chem.*, 2002, **12**, 1423–1425.
- H. Ehrenberg, M. Wiesmann, J. Garcia-Jaca, H. Weitzel and H. Fuess, *J. Magn. Magn. Mater.*, 1998, **182**, 152–160.
- J. Zhao, Q.-S. Wu and M. Wen, *J. Mater. Sci.*, 2009, **44**, 6356–6362.
- A. P. De Moura, L. H. De Oliveira, P. F. S. Pereira, I. L. V. Rosa, M. S. Li, E. Longo and J. A. Varela, *ACES*, 2012, **2**, 465–473.
- P. Schmitt, N. Brem, S. Schunk and C. Feldmann, *Adv. Funct. Mater.*, 2011, **21**, 3037–3046.
- M.-C. Liu, L.-B. Kong, X.-J. Ma, C. Lu, X.-M. Li, Y.-C. Luo and L. Kang, *New J. Chem.*, 2012, **36**, 1713–1716.
- C. Peng, L. Gao, S. Yang and J. Sun, *Chem. Commun.*, 2008, 5601–5603.
- W. Xiao, J. S. Chen, C. M. Li, R. Xu and X. W. Lou, *Chem. Mater.*, 2010, **22**, 746–754.
- Y. Ding, Y. Wan, Y.-L. Min, W. Zhang and S.-H. Yu, *Inorg. Chem.*, 2008, **47**, 7813–7823.
- K. Eda, Y. Uno, N. Nagai, N. Sotani and M. Stanley Whittingham, *J. Solid State Chem.*, 2005, **178**, 2791–2797.
- K. Eda, Y. Uno, N. Nagai, N. Sotani, C. Chen and M. Stanley Whittingham, *J. Solid State Chem.*, 2006, **179**, 1453–1458.
- A. Rodriguez, S. Chaturvedi, J. C. Hanson, A. Albornoz and J. L. Brito, *J. Phys. Chem. B*, 1998, **102**, 1347–1355.
- L. Righetti, L. Robertson, A. Largeau, G. Vignoles, A. Demourgues and M. Gaudon, *ACS Appl. Mater. Interfaces*, 2011, **3**, 1319–1324.
- A. Patterson, *Phys. Rev.*, 1939, **56**, 978–982.
- C. N. R. Rao, F. L. Deepak, G. Gundiah and A. Govindaraj, *Prog. Solid State Chem.*, 2003, **31**, 5–147.
- M. T. Dove, *Am. Mineral.*, 1997, **82**, 213–244.